JOURNAL OF PROPULSION AND POWER
Vol. 16, No. 6, November–December 2000

Soot Patterns Around Suspended *n*-Heptane Droplet Flames in a Convection-Free Environment

C. Thomas Avedisian*
Cornell University, Ithaca, New York 14853-7501
and
Gregory S. Jackson†
University of Maryland, College Park, Maryland 20742

The trapping and transport of soot aggregates between a burning suspended droplet and its flame in a convection-free (microgravity) environment are discussed. Many researchers have utilized the suspended droplet method for studying droplet combustion in microgravity where the intent is to create a spherically symmetric burning process. In the ideal case, soot particles are trapped in a spherical shell-like structure between the droplet and the flame. Results presented show that the fiber support can prevent the formation of spherical soot shells if the fiber diameter is large relative to the droplet diameter are presented for suspended droplets burning in microgravity. The effect of the fiber is conjectured to arise by its influence on the gas-phase temperature and Stefan velocity fields around the burning droplet. Droplets with initial diameters between 700 and 850 θm were mounted on silica quartz fibers with diameters of 57, 110, 220, and 330 θm, and the droplets were ignited with sparks generated from two retractable electrode pairs. Photographic records of the burning process show soot aggregates inside the flame forming a shell-like structure, which evolves into a nonsymmetric configuration due to a nonsymmetric distribution of thermophoretic and Stefan drag forces around the droplet caused by flame/fiber interactions. For the four fiber diameters examined, the burning rates (extracted over a large portion of burning process) appear to approach the free droplet value as the ratio of the initial droplet diameter to the fiber diameter increases.

I. Introduction

DROPLET combustion has long been studied to gain insights into liquid fuel burning processes in power and propulsion devices. Single-isolated droplet combustion experiments have often implemented a technique where the droplet is anchored or suspended at the tip of a single fiber or at the center of a stretched fiber and then burned in a microgravity environment. Observations from studies of suspended droplets burning in microgravity have provided much of the current understanding of spherically symmetric droplet burning, an often-made assumption for modeling complex droplet burning processes. The suspended droplet technique continues to be used in contemporary studies of droplet burning of sooting fuels carried out in microgravity at both normal[1–3] and elevated[4–6] pressures.

A support fiber can have some undesirable effects on the burning process. It can distort the droplet shape and enhance conduction heat transfer from the flame to the droplet. These effects have been known since the early days of droplet combustion experimentation,[7,8] and procedures to compensate for them have been proposed. The effects should diminish as the initial droplet diameter d_0 increases relative to the fiber diameter d_{fiber}. Because the droplet diameter d decreases during burning (in the following the term droplet diameter is understood to mean an equivalent diameter of the nonspherical suspended droplet), the fiber will always affect burning near the end because $d/d_{\text{fiber}} \to 0$. Maximizing d_0/d_{fiber} allows for the greatest fraction of the burning process to mimic that of a free droplet.

One aspect of the suspended droplet technique that has not been addressed is the influence of the fiber on the transport and entrapment of soot aggregates inside the droplet flame, particularly under microgravity conditions where buoyancy-induced flows are small. In this paper, we present photographic records that show that the fiber can significantly impact soot entrapment patterns.

Received 24 February 1999; revision received 4 August 1999; accepted for publication 20 August 1999.

*Professor, Sibley School of Mechanical and Aerospace Engineering.
†Assistant Professor, Department of Mechanical Engineering.

Soot particles formed during combustion of fuel droplets are trapped between the droplet and flame. The resulting shell, noticed in early studies by Kobayashi[9] under normal gravity and by Kumagai et al.[10] for microgravity droplet flames, arises when the forces on the particles due to gas-phase flows and thermophoresis balance to trap them between the droplet and flame.[11–13] For a suspended droplet in a stagnant far-field gas, flow arises because of natural convection and the evaporation process itself (so-called Stefan flow). At normal gravity, buoyant flows tend to dominate over Stefan flows, and soot particles are trapped in tracks that follow the shape of the wake flame and show little influence from the support fiber regardless of the fiber diameter. At low gravity, the Stefan flow dominates and pushes the soot aggregates radially outward toward the flame until the inwardly directed thermophoretic force, which is proportional to the gas-phase temperature gradient,[14] counterbalances the outwardly directed drag force. The aggregates become trapped and produce a dark ring or shell surrounding the droplet (see Avedisian[15] for a discussion and review of the history of this problem). However, as presented in this paper, soot aggregates are not necessarily trapped symmetrically around a suspended droplet burning in a stagnant ambiance in microgravity. Flame/fiber interactions can produce axisymmetric (but not spherically symmetric) gas flow and temperature fields around the droplet that upset the spherical symmetry of the burning process.

To show the effect of the fiber on the soot patterns, suspended *n*-heptane droplets were anchored on the tip of a vertically oriented fine quartz fiber and then burned in microgravity using a drop tow facility. (An alternative droplet support technique is to mount the droplet onto a stretched fiber as was done by Lebedev and Marchenko[16] and later by Dietrich.[17] The flame would then intersect the fiber at two points on opposite sides of the droplet, which may reduce temperature asymmetries and promote more symmetric burning.) Because of the extensive use of *n*-heptane as a fuel in prior microgravity droplet combustion experiments, results of the present study could be compared with previously observed free droplet burning rates and soot patterns.[1] Four fiber diameters were used: 57, 110, 220, and 330 μm. The mass of fuel placed on each fiber was approximately the same to provide a basis of comparison. A two-spark

retractable electrode arrangement provided the energy to initiate the burning process with minimal disturbance to the droplet and gas field.

The patterns and transport of soot aggregates around the burning droplets were recorded using high-speed cine photography with back lighting set to emphasize the characteristics of the soot shell. More quantitative methods such as those involving laser diagnostics[3,18] have also been used to study soot inside suspended droplet flames in microgravity, but such methods were not used here as they would not have provided substantially more information relevant to this study. Frame by frame analysis of the motion picture sequences provided data on the evolution of droplet diameter during the burning process.

II. Experiment

The suspended droplet experiments were conducted in a drop-tower facility described previously.[1,11,19,20] Approximately 1.2 s of free fall was available, which restricted droplet sizes to less than 1 mm for observing the complete burning history in the low-gravity environment at atmospheric pressure. The gravity level was about $10^{-4} g/g_0$ (where $g_0 = 9.8$ m/s^2) in the moving frame of reference because a drag shield was used. The droplets were suspended from fused silica (quartz) fibers that were modified from fiber optic cables. To anchor the droplet, a small spherical bead about twice the fiber diameter was placed at the end of fibers by a fine acetylene torch.

Droplets were deployed on the support fibers by generating two consecutive droplets from a piezoelectric droplet generator upward so that they impinged onto the support fiber just above the bead. If more than one droplet was needed to build up the size of interest, they were directed to impinge onto the hanging droplet. Figure 1 is a schematic of the deployment process. The volume of one individual droplet produced from the generator was approximately 0.065 mm^3. Ignition was by a two-spark arrangement. The electrode gaps (about 3 mm) were placed on opposite sides of the droplet about 2 mm from the droplet center and at the plane of the supported droplet center. Spark energies and durations of about 0.11 J and 0.50 ms, respectively, were used to ignite the suspended droplets. The energy and duration were kept to a minimum to reduce disturbances of the gas surrounding the droplet by the spark impulse.

The experimental procedure involved deploying the droplet by the aforementioned method and then releasing the instrumentation package with its drag shield into free fall. The sparks were activated to ignite the supported droplet approximately 5 ms after separation of the package from the electromagnet, which held the package in place before free fall. For each fiber size, between four and five experiments were carried out to show the repeatability of the burning process and soot patterns formed. Prior to each experiment the fiber was either cleaned of soot residue or replaced by a new fiber.

Burning histories were recorded at 200 frames/s by a Redlake LOCAM 2 16-mm movie camera with an Olympus Zuiko 90-mm macrolens. The interest here was on observing the droplet and soot, with the outer luminous flame zone being of secondary importance. It is difficult to obtain high-quality photographs of all three simultaneously, and thus, backlighting was adjusted to provide clear images of both the droplet and soot at the expense of flame visibility. The distance from the front of the lens to the suspended droplet was about 90 mm, which gave a reproduction ratio of about 1 : 1 and a field of view of about 2 mm. Figure 2 shows representative prints from the motion picture sequences that illustrate the visibility of both the droplet and soot patterns formed. The free-droplet sequence is from Jackson and Avedisian.[1] The suspended droplet photographs show the effect of the fiber diameter on soot, which are the dark ring patterns. Figure 2b shows three enlargements at selected times for the 110 μm support. These images are discussed further in the next section.

III. Data Reduction

Droplet diameters were obtained from a frame-by-frame analysis of the movie films using a frame grabber board on a Macintosh and image analysis software from Automatics. Various approximations for determining d from the individual images have been used that account for the nonspherical shape of the supported droplet. Methods include measuring maximum horizontal dimension, taking a dimension at 45 deg to the fiber axis,[10] averaging distances to the droplet edge from a calculated droplet centroid,[1] or assuming an ellipsoid shape to fit the boundary of the droplet and calculating a diameter for an equivalent volume.[8–10] Differences in these methods are most significant for droplets supported on large diameter fibers (such as the 330 μm fibers in this study); methods based on equivalent liquid volume, however, were found to give the most consistent burning rates for droplets supported on the large-diameter fibers. Thus, the ellipsoid volume method, which has been commonly used in previous studies, was adopted for this study.

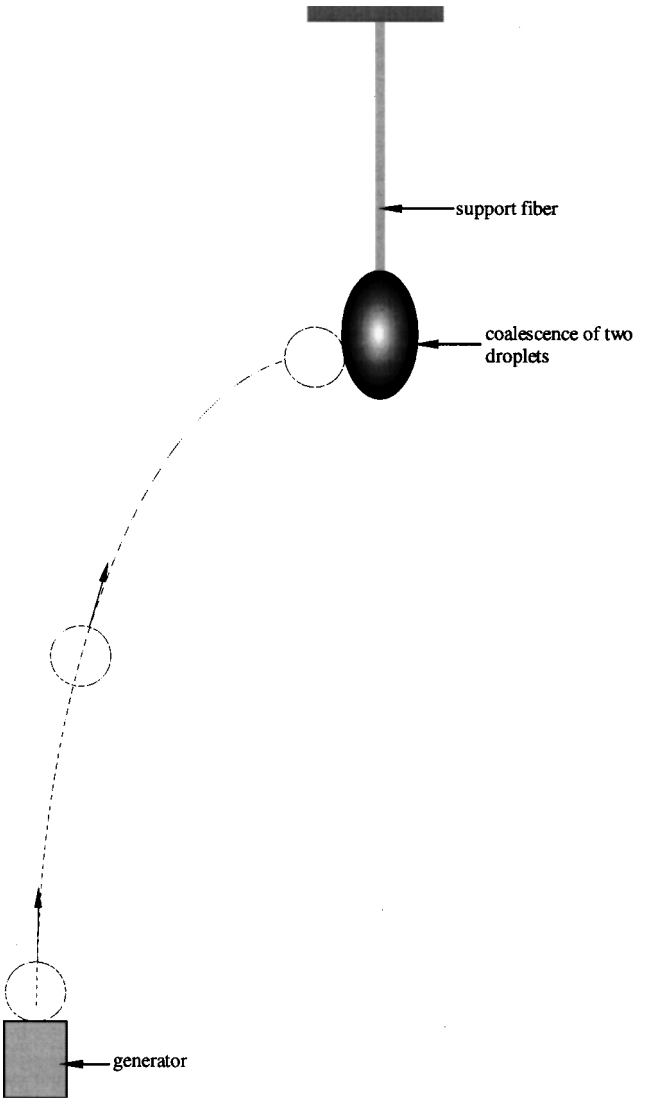

Fig. 1 Schematic of droplet deployment onto a support fiber.

Digitized droplet images were analyzed by determining the droplet/gas boundary with an appropriate gray scale setting and then calculating the liquid volume corresponding to a body of revolution defined by the profile boundary of the droplet. The volume of revolution V_{rev} was calculated from a curve fit describing the shape of the droplet boundary. For the calculation, the liquid volume was assumed to intersect the fiber as a smooth continuation of the droplet surface, and the meniscus at the droplet/fiber interface was not included in the volume calculations. The equivalent droplet diameter, as expressed in Eq. (1), was defined as the diameter that gave the equivalent volume as $V = V_{rev} - V_{fiber}$, where V_{fiber} is the volume of the fiber encircled by the volume of revolution V_{rev}:

$$d = \sqrt[3]{6V/\pi} \tag{1}$$

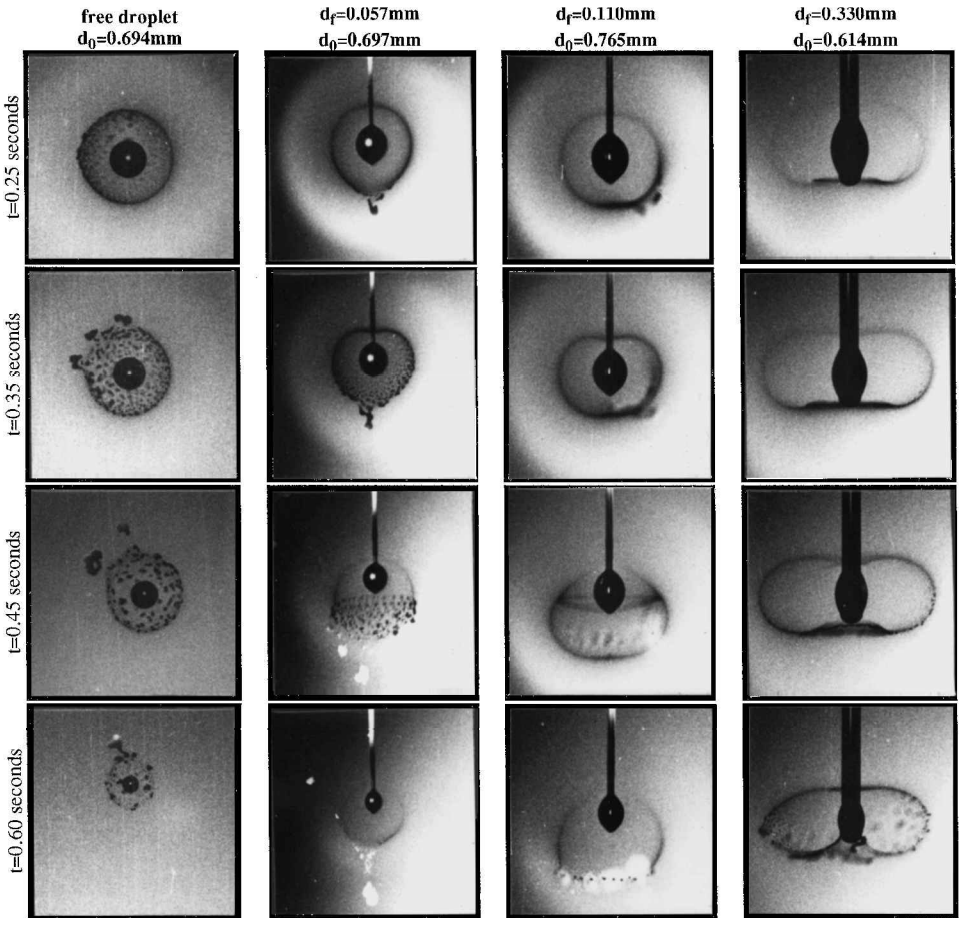

Fig. 2a Photographs showing patterns of soot aggregate trapping for *n*-heptane droplets suspended from quartz fibers with 57-, 110-, and 330-θ m diameter.

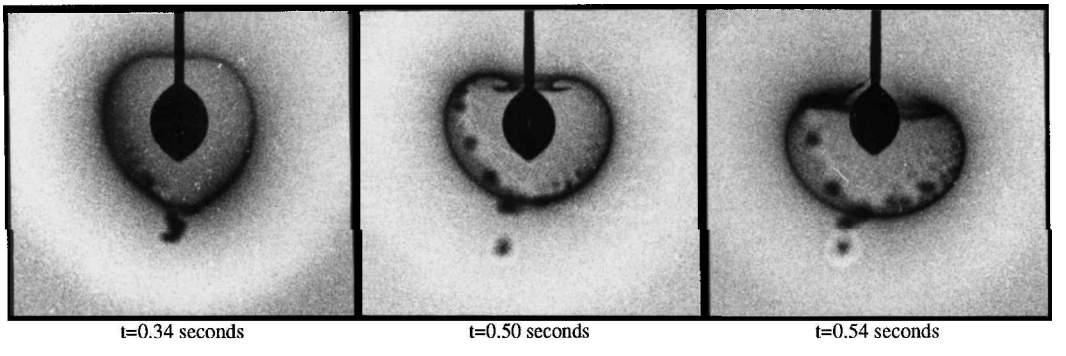

Fig. 2b Detail of evolution of the soot vortex at the droplet surface due to downward sweeping of soot aggregates; times shown are after ignition; droplet flame out of field of view.

This definition of equivalent droplet diameter allowed the equivalent droplet diameter to approach zero as the liquid was evaporated during burning.

The evolution of equivalent diameter was found to be qualitatively similar for the fiber sizes examined, but produced different quantitative values of the burning rate K defined as

$$K \equiv -\frac{\mathrm{d}(d^2)}{\mathrm{d}t} \tag{2}$$

As will be noted in Sec. IV, the burning records did not show precisely constant rates, or linear variations of equivalent diameter with time, over the entire period of burning. Especially near the end of burning for the larger fiber diameters, K increased sharply, which may be both an artifact of the definition of d and an indication of enhanced heat transfer to the droplet from the fiber. To determine K from Eq. (2), data only over the most linear portion of the evolution of diameter were used as noted subsequently.

IV. Results and Discussion

Figure 2 shows photographs of the droplet, the support fiber, and soot formations around the droplet. The photographic records illustrate the dynamic nature of soot entrapment and the evolution of droplet shape. The first column of Fig. 2a is a free droplet[1] for comparison with the other columns showing droplets suspended on fibers of various diameters. The computed initial droplet diameters are indicated along the top row, whereas time after ignition is given on the left. Times shown are after ignition. The flame is visible in some of the photographs.

Early in the droplet burning, the balance of Stefan and thermophoretic forces trap soot aggregates inside the flame. For the

smaller fibers ($d_{\text{fiber}} = 57$ or 110 μm), the trapping of soot is relatively symmetric around the droplet early in the burning process ($t < 0.30$ s). Although the photographs indicate a relatively narrow dark ring of soot particles, soot particle locations are not so sharply defined because the range of particle sizes causes a variation in the radial position where the thermophoretic and Stefan drag forces balance.[12] As the burning process continues and the droplet diameter decreases, the role of the fiber on the velocity and temperature fields around the droplet begins to upset the symmetry of the soot particles. The disruption of the soot shell, as illustrated in the photographic sequences for the 57- and 110-μm fibers, is signified by an inward collapse of the soot shell above the droplet and the expansion of the soot shell and emission of large soot particles beneath the droplet away from the fiber. The emission of larger soot aggregates is similar to that observed during the free droplet burning, where the soot shell remains spherical except for the large aggregates that drift out of the soot shell and through the flame. The outward motion of the large soot aggregates is due to the outward Stefan drag force increasing more rapidly with particle size than the inward thermophoretic force.[12]

For the largest fiber diameters (330 μm), the spherical symmetry of the soot shell structure was distorted as soon as the soot particles began to collect around the droplet very early in the burning process. The effects of the large-diameter fiber on the gas-phase temperature and flowfields resulted in elongation of the soot shell perpendicular to the fiber and compression of the soot shell along the axis of the fiber, as indicated in Fig. 2a. The lack of significant vaporization beneath the fiber may have contributed to the inward movement of soot particles along the axis of the fiber and the apparent anchoring of aggregates to the tip of the fiber.

The observed structure and dynamics of the soot particles inside the droplet flame indicate that the soot particles in the shell structure have a collective bubblelike quality. A relatively uniform movement of particles in the downward and outward direction away from the fiber results in an opening of the shell in some cases ($d_{\text{fiber}} = 57$ μm, $t = 0.45$ s; $d_{\text{fiber}} = 110$ μm, $t = 0.60$ s). The downward and outward movement of soot particles forms a rim from which larger soot aggregates are emitted into the high-temperature flame zone as evidenced by the intense (white) radiation from the particles. Interestingly, for $d_{\text{fiber}} = 57$ μm, the shell closes again ($t = 0.60$ s), but in the case of $d_{\text{fiber}} = 110$ μm, the shell remains open while continuing to emit aggregates.

In the region above a burning suspended droplet, the soot shell moved downward axisymmetrically toward the droplet/fiber interface. The downward motion suggests that the thermophoretic force was comparatively stronger than the Stefan drag force along the axis of the fiber. This may in part be because, near the fiber, Stefan velocities at the meniscus primarily directed outward from the fiber. On the

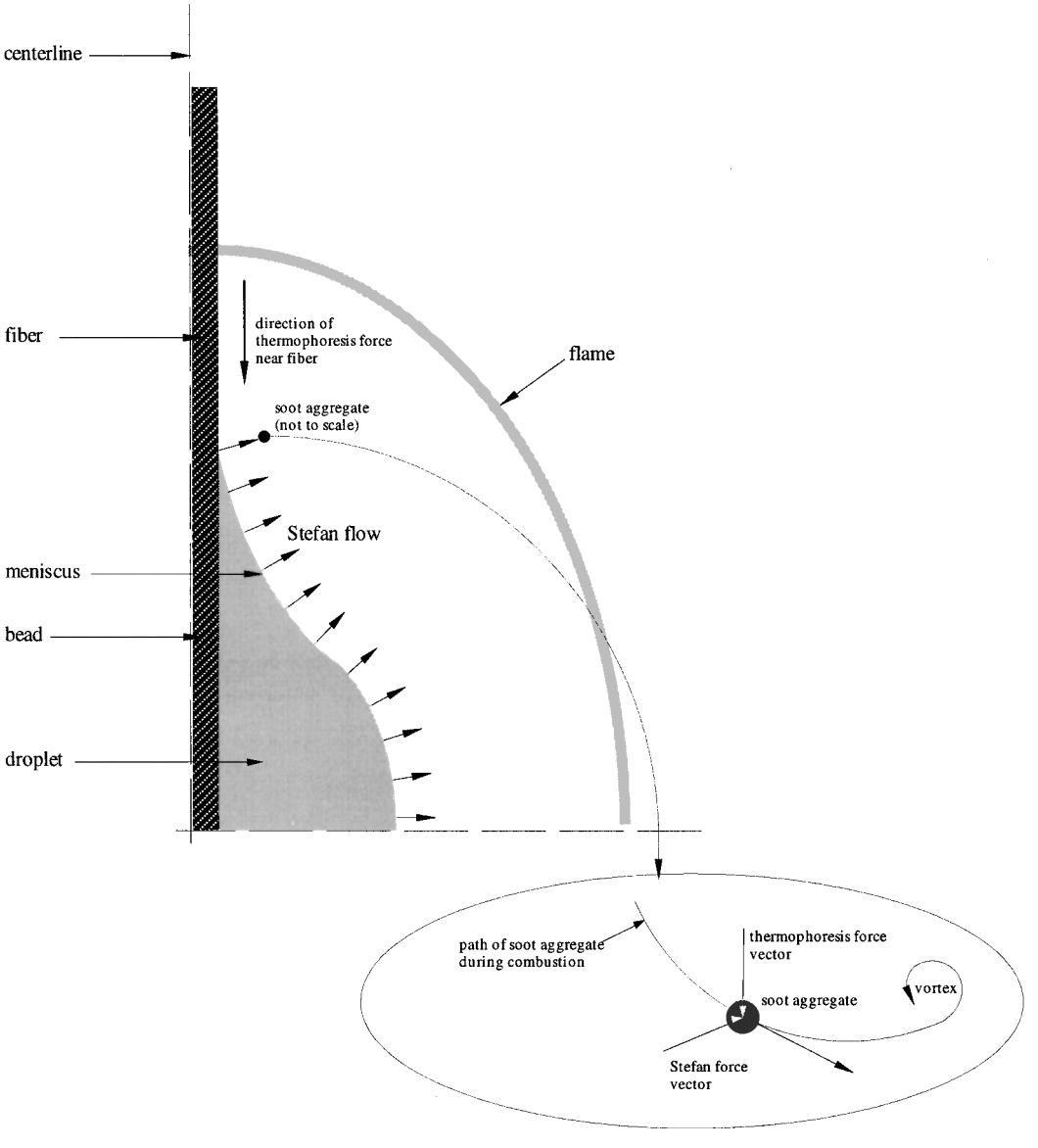

Fig. 3 Forces acting on soot aggregates near to the liquid meniscus that can lead to formation of soot vortex.

other hand, the flame structure was likely to create thermophoretic forces acting inward toward the droplet along the axis of the fiber near the meniscus. The net combination of these two force fields on the soot particles above the droplet could result in soot particle trajectories that follow a downward and then outward motion in a vortexlike pattern as suggested in Fig. 2b, $t = 0.50$ s. Figure 3 schematically illustrates the postulated processes near the fiber. As burning proceeded, the soot vortex moved down around the drop and formed a ring of large aggregates ($t = 0.45$ s, $d_{\text{fiber}} = 110\ \mu$m in Fig. 2a; $t = 0.54$ s in Fig. 2b) that appeared like a moving wave in the motion picture film. These soot patterns are only visible when the backlighting is not so intense that it overrides the luminosity due to oxidation of the soot.

Other visualization methods can be used to infer the symmetry of droplet burning in microgravity. For example, probing the lower hemisphere around a suspended dodecane droplet using a planar laser scattering technique,[18] with initial droplet diameter around 1000 μm and a fiber diameter of 250 μm (giving $d_0/d_{\text{fiber}} = 4$), indicated evidence of a spherical soot pattern for the hemisphere that could be visualized. This result is consistent with the photographs in Fig. 2a for d_0/d_{fiber} in this same range (third and fourth columns in Fig. 2a) that show a spherical shell structure early in the burning history. However, for $d_{\text{fiber}} = 110\ \mu$m ($d_0/d_{\text{fiber}} = 6.95$), the upper hemisphere where the fiber's effects were strongest indicated a distorted soot shell.

Figure 4 shows measurements of the evolution of the droplet diameter for the four fiber diameters examined. The data in Fig. 4 show the repeatability of the results. For $d_{\text{fiber}} = 57\ \mu$m the droplet diameter decreases almost to zero, whereas for the 330 μm fiber only about 80% of the burning history is indicated. This latter result is an artifact of the difficulty of defining the liquid mass on the large fiber near the end of burning and of curve fitting the profile shape. For each fiber diameter, the variation of diameter with time shows a linear portion.

Significant nonlinearity in the evolution of diameter exists for the data in Fig. 4, especially for the largest fiber diameter near the end of burning. Notwithstanding this, to show qualitative trends of the burning process with fiber diameter, we extracted a burning rate from each data set as a single average value over the portion of the burning history where the evolution of equivalent droplet diameter was most linear. The arrows superimposed on Fig. 4 indicate the linear region of the data that was used for determining the burning rates from Eq. (2). Although this procedure is approximate and the results do not capture detailed processes that influence the burning history, the results still show in a simple way how the fiber influences burning for the data reported here. Figure 5 shows the variation of average burning rate K_{fiber}, with normalized equivalent initial droplet diameter d_0/d_{fiber}. The abscissa is normalized by measured unsupported droplet burning rates K_{free} for heptane, which were obtained from Ref. 1 corresponding to the d_0 of the fiber supported droplet. The line is drawn to suggest the trend that as d_0/d_{fiber} increases, K_{fiber} approaches K_{free}, as might be expected. For $d_0/d_{\text{fiber}} \geq 13$ (corresponding to the droplets supported on the 57-μm fiber in this study), the supported droplet burning rate is

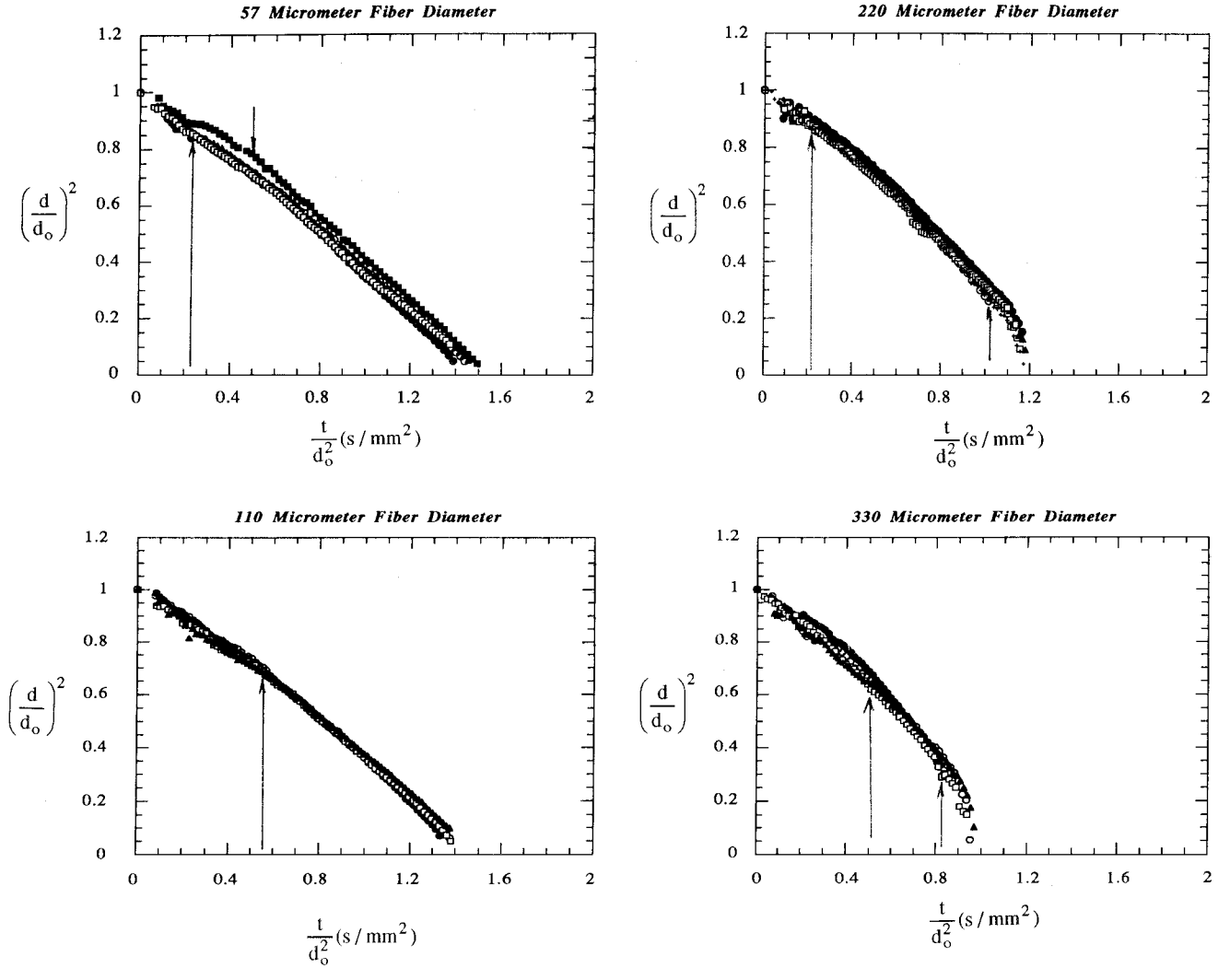

Fig. 4 Evolution of diameter for droplets on quartz fibers of the indicated diameters; data between arrows were used to obtain burning rates from a linear curve fit.

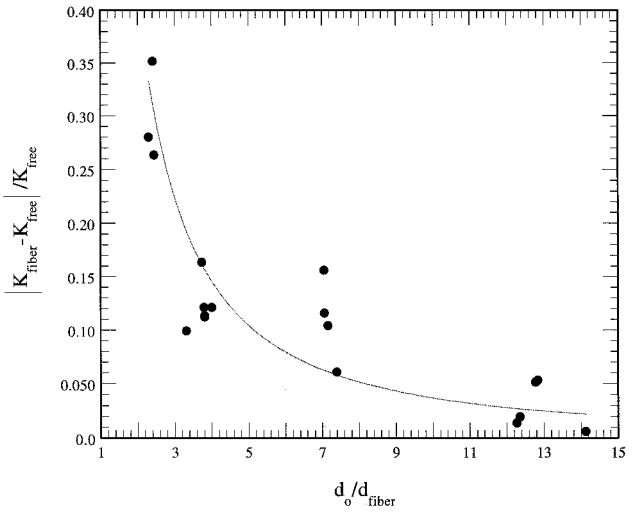

Fig. 5 Variation of nondimensional burning rate obtained from linearizing the data shown in Fig. 4. K_{free} values obtained from Ref. 1 for d_0 values of data in Fig. 4; line is drawn to suggest a trend.

basically the same as the free droplet value in the most linear portion of burning in spite of the fact that the soot shell is not spherical as shown in Fig. 2.

V. Conclusions

Soot patterns around *n*-heptane droplets suspended from the tip of a fiber in microgravity showed deviations from spherical symmetry that depended on the ratio of droplet and fiber diameter. And the shell-like structure formed by trapped soot aggregates exhibited shapes which varied with time during the droplet burning process. In some cases downward movement of soot aggregates was observed in which the shell opened up and aggregates were emitted through the flame and away from the fiber tip. In other cases, motion of the aggregates along the fiber axis created a vortex-like pattern as the shell moved along the fiber and around the droplet. These asymmetries in soot patterns are attributed to asymmetric temperature and velocity fields in the gas phase around the drop arising from flame/fiber interactions that caused asymmetries in the Stefan and thermophoretic forces acting on the soot particles.

For $d_0/d_{fiber} > 13$, the fiber supported burning rates, measured over the most linear portion of the evolution of droplet diameter, are close to the free droplet value. For smaller ratios of d_0/d_{fiber}, the burning rate increased, and the fractional change in the burning rate increased as d_0/d_{fiber} decreased.

Acknowledgments

This project was supported by NASA through Grant NAG 3-1971 (Merrill King, Director and Daniel Dietrich, Project Monitor). The authors thank John Wellin for his help with the experiments and data analysis.

References

[1]Jackson, G. S., and Avedisian, C. T., "Experiments on the Effect of Initial Diameter in Spherically Symmetric Droplet Combustion of Sooting Fuels," *Proceedings of the Royal Society of London, Series A: Mathematical and Physical Sciences*, Vol. 446, 1994, pp. 251–278.

[2]Aharon, I., "Theoretical and Experimental Studies of Evaporation and Combustion of Multicomponent Droplets in Reduced Gravity," Ph.D. Dissertation, Univ. of California, Davis, CA, 1996.

[3]Choi, M. Y., and Lee, K.-O., "Investigation of Sooting in Microgravity Droplet Combustion," *Twenty-Sixth Symposium (International) on Combustion*, Combustion Inst., Pittsburgh, PA, 1996, pp. 1243–1249.

[4]Mikami, M., Kono, M., Sato, J., Dietrich, D. L., and Williams, F. A., "Combustion of Miscible Binary-Fuel Droplets at High Pressure Under Microgravity," *Combustion Science and Technology*, Vol. 90, 1993, pp. 111–123.

[5]Chauveau, C., Chesneau, X., and Gokalp, I., "Burning Characteristics of N-Heptane Droplets Under Different Regimes," AIAA Paper 93-0824, 1993.

[6]Sato, J., Tsue, M., Niwa, M., and Kono, M., "Effects of Natural Convection in High Pressure Droplet Combustion," *Combustion and Flame*, Vol. 82, 1990, pp. 142-150.

[7]Godsave, G. A. E., "Combustion of Droplets," *Nature*, Vol. 166, 1950, p. 1111.

[8]Godsave, G. A. E., "Studies of the Combustion of Drops in a Fuel-Spray—The Burning of Single Drops of Fuel," *Fourth Symposium (International) on Combustion*, Combustion Inst., Pittsburgh, PA, 1953, pp. 818–830.

[9]Kobayashi, K., "An Experimental Study of the Combustion of a Fuel Droplet," *Third Symposium (International) on Combustion*, Combustion Inst., Pittsburgh, PA, 1955, pp. 141–148.

[10]Kumagai, S., Sakai, T., and Okajima, S., "Combustion of Free Fuel Droplets in a Freely Falling Chamber," *Proceedings of the Thirteenth Symposium (International) on Combustion*, Combustion Inst., Pittsburgh, PA, 1971, pp. 779–785.

[11]Jackson, G. S., Avedisian, C. T., and Yang, J. C., "Observations of Soot in Droplet Combustion at Low Gravity: Heptane and Heptane/Monochloroalkane Mixtures," *International Journal of Heat and Mass Transfer*, Vol. 35, 1992, pp. 2017–2033.

[12]Jackson, G. S., and Avedisian, C. T., "Modeling Spherically Symmetric Droplet Flames Using Complex Chemistry: Effects of Droplet Size and Water Addition on *n*-Heptane Droplet Combustion," *Combustion Science and Technology*, Vol. 115, 1996, pp. 127–147.

[13]Choi, M. Y., Dryer, F. L., Green, G. J., and Sangiovanni, J. J., "Soot Agglomeration in Isolated, Free Droplet Combustion," AIAA Paper 93-0823, 1993.

[14]Talbot, L., Cheng, R. K., Schefer, R. W., and Willis, D. R., "Thermophoresis of Particles in a Heated Boundry Layer," *Journal of Fluid Mechanics*, Vol. 101, 1980, pp. 737–758.

[15]Avedisian, C. T., *Physical and Chemical Aspects of Combustion*, Gordon and Breach, New York, Chap. 6, 1997, pp. 135–160.

[16]Lebedev, O. N., and Marchenko, V. N., "An Experimental Study of Vaporization of Droplets of Hydrocarbon Fuels at High Gas Temperatures and Presssures," *Heat Transfer—Soviet Research*, Vol. 11, No. 3, 1979, pp. 92–98.

[17]Dietrich, D. L., and Haggard, J. B., "Combustion of Interacting Droplet Arrays in a Microgravity Environment," *Second International Microgravity Combustion Workshop*, CP-10113, NASA, 1992, pp. 317–323.

[18]Tsue, M., Segawa, D., Kadota, T., and Yamasaki, H., "Observations of Sooting Behavior in an Emulsion Droplet Flame by Planar Laser Light Scattering in Microgravity," *Proceedings of the Twenty-Sixth Symposium (International) on Combustion*, Combustion Inst., Pittsburgh, PA, 1996, pp. 1251–1258.

[19]Avedisian, C. T., Yang, J. C., and Wang, C. H., "On Low Gravity Droplet Combustion," *Proceedings of the Royal Society of London, Series A: Mathematical and Physical Sciences*, Vol. 420, 1988, pp. 183–200.

[20]Jackson, G. S., and Avedisian, C. T., "Combustion of Unsupported Water-in-Heptane Emulsion Droplets in a Convection-Free Environment," *International Journal of Heat and Mass Transfer*, Vol. 41, No. 16, 1998, pp. 2503–2515.